The array invariant

Sunwoong Lee[a] and Nicholas C. Makris[b]
Massachusetts Institute of Technology, Department of Mechanical Engineering, Cambridge, Massachusetts 02139

(Received 16 February 2005; revised 14 August 2005; accepted 17 October 2005)

A method is derived for instantaneous source-range estimation in a horizontally stratified ocean waveguide from passive beam-time intensity data obtained after conventional plane-wave beamforming of acoustic array measurements. The method has advantages over existing source localization methods, such as matched field processing or the waveguide invariant. First, no knowledge of the environment is required except that the received field should not be dominated by purely waterborne propagation. Second, range can be estimated in real time with little computational effort beyond plane-wave beamforming. Third, array gain is fully exploited. The method is applied to data from the Main Acoustic Clutter Experiment of 2003 for source ranges between 1 to 8 km, where it is shown that simple, accurate, and computationally efficient source range estimates can be made. © *2006 Acoustical Society of America.* [DOI: 10.1121/1.2139074]

PACS number(s): 43.60.Fg, 43.60.Jn, 43.30.Bp [WLS] Pages: 336–351

I. INTRODUCTION

It has long been known that multi-modal dispersion in a shallow water waveguide degrades the performance of bearing estimates by conventional plane-wave beamforming. This is due to the advent of spurious effects unique to the waveguide environment, such as multiple peaks and beam spreading in the beamformer output.[1–3] Attempts, on the other hand, have been made to localize sources submerged in ocean waveguides by exploiting multi-modal interference using methods such as matched field processing (MFP).[4–6] Apart from being computationally expensive, MFP techniques require accurate knowledge of the wave propagation environment. They are susceptible to large systematic errors from mismatch when adequate environmental information is not available.[7,8]

The range of a source in a horizontally stratified ocean waveguide can sometimes also be estimated by the much simpler waveguide invariant method,[9–11] which employs only incoherent processing of acoustic intensity data as a function of range and bandwidth. The waveguide invariant method, however, requires knowledge of certain "invariant" parameters, which unfortunately often vary significantly with ocean sound speed structure. It also requires a sufficiently large number of waveguide modes to significantly contribute to the measured field because these cause the interference structure necessary to produce a unique solution. Sufficiently dense sampling of the intensity data in source-receiver range is also necessary to provide an unambiguous solution. When the application involves single-sensor measurements, joint ambiguity in source-receiver range and velocity is an inherent limitation of the waveguide invariant method. This ambiguity can disappear when spatial sensor arrays of sufficient horizontal aperture are used. None of the usual benefits of increased signal-to-noise ratio at the array output appear, however, because only incoherent processing of the spatial samples can be performed.

Here we show that instantaneous source range estimation is possible in a horizontally stratified ocean waveguide by a computationally inexpensive method that has significant advantages over the waveguide invariant because it requires neither *a priori* knowledge of environmental parameters nor multiple modes in the received field, and fully exploits the coherent gain possible with receivers of finite spatial aperture.[12] Since the new approach takes advantage of invariant properties of passive beam-time intensity data obtained after conventional plane-wave beamforming of underwater acoustic array measurements, we call it the *array invariant* method. We show that maximum beam-time intensity migrates along an angle that is invariant to environmental parameters but follows a known and unique dependence on source-receiver range. Horizontal source localization is also achieved when the receiving array has sufficient horizontal aperture to resolve source bearing. The formulation introduced here is specifically for broadband transient source signatures. A more general but involved formulation that can treat continuous broadband noise signatures is possible.[13]

The array invariant method is derived in Sec. II. Illustrative examples are presented in Sec. III. In Sec. IV, source localization by the array invariant method is experimentally demonstrated using data from the Main Acoustic Clutter 2003 Experiment (MAE). Comparisons between the array invariant method and other acoustic techniques for source range estimation in the ocean, such as the waveguide invariant method and MFP, are presented in Sec. V.

II. DERIVATION OF THE ARRAY INVARIANT

Analytic expressions are derived for the migration of peak intensity through a beam-time intensity image generated from acoustic array measurements made in an ideal waveguide. It is then shown that the expressions are approxi-

[a]Electronic address: sunwoong@mit.edu
[b]Electronic address: makris@mit.edu

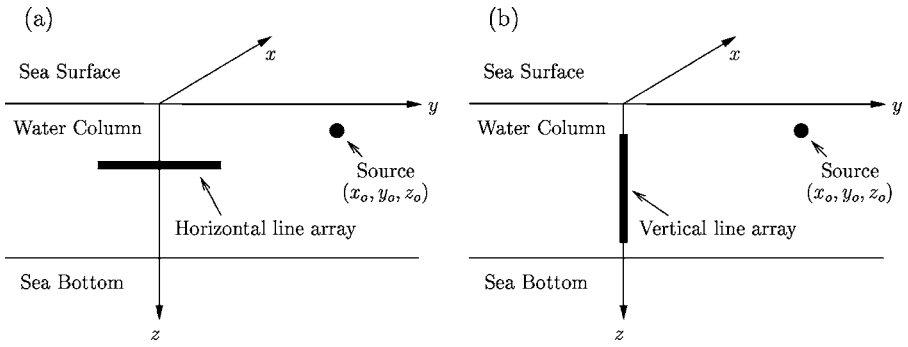

FIG. 1. The geometry of the coordinate system for a horizontal line array (a), or a vertical line array (b). The horizontal line array is aligned parallel to the y-axis. The vertical line array is located along the z-axis. A source is located at (x_o, y_o, z_o).

mately valid for typical horizontally stratified ocean waveguides, where they can be used for instantaneous source localization.

A. Beam-time migration for horizontal arrays in stratified waveguides

The measurement and coordinate geometry of Fig. 1(a) shows a horizontal line array parallel to the y axis, with array center at $(0,0,z)$, and source at (x_o, y_o, z_o). We define $\mathbf{r} = x\hat{i}_x + y\hat{i}_y$, and $r = |\mathbf{r}|$, where $\hat{i}_x$ and $\hat{i}_y$ are unit vectors in the x and y directions, respectively. The wavenumber vector $\mathbf{k}$ is decomposed into $k_x = -k \sin\phi \cos\theta$, $k_y = -k \sin\phi \sin\theta$, and $k_z = -k \cos\phi$, where $k = |\mathbf{k}|$, and elevation angle ϕ and bearing θ are shown in Fig. 2.

The pressure P at frequency f due to a source at $(\mathbf{r_o}, z_o)$ can be expressed using normal mode theory as

$$P(\mathbf{r},z,f) = 4\pi Q(f) \frac{i}{\sqrt{8\pi\rho(z_o)}} e^{-i\pi/4} \times \sum_n u_n(z_o) u_n(z) \frac{e^{ik_{rn}|\mathbf{r}-\mathbf{r_o}|}}{\sqrt{k_{rn}|\mathbf{r}-\mathbf{r_o}|}}, \quad (1)$$

where $Q(f)$ is the source spectrum, ρ is the density, k_{rn} is the horizontal wavenumber of the nth mode, and u_n is the mode shape of the nth mode which satisfies $\int_0^\infty u_m(z) u_n^*(z)/\rho(z) dz = \delta_{mn}$. Using the far-field approximation $|\mathbf{r}-\mathbf{r_o}| \simeq r_o - y \sin\theta_o$, where θ_o is source bearing, the beamformed pressure P_B can be expressed as a function of array scan angle θ,

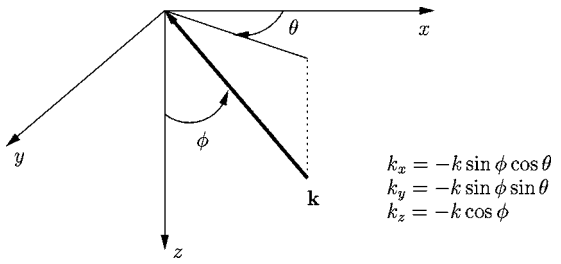

FIG. 2. Definition of the elevation angle ϕ and the bearing θ of plane waves. The angles are defined in the "coming from" direction.

$$P_B(s,f) = \int_{-\infty}^{\infty} T(v) P(v,z,f) e^{i2\pi v \sin\theta} dv = 4\pi Q(f) \frac{i}{\sqrt{8\pi\rho(z_o)}} e^{-i\pi/4} \times \sum_n u_n(z_o) u_n(z) \frac{e^{ik_{rn}r_o}}{\sqrt{k_{rn}r_o}} B(s-s_n), \quad (2)$$

where $s = \sin\theta$, $v = ky/2\pi$, $s_n = \sin\phi_n \sin\theta_o$, and $\sin\phi_n = k_{rn}/k$. For evanescent modes, $\phi_n = \pi/2 - i\phi_n'$ where $\phi_n' = \ln[k_{rn}/k + \{(k_{rn}/k)^2 - 1\}^{(1/2)}]$. The beam pattern $B(s)$ is the spatial Fourier transform of the array taper function $T(v)$.[14] This far-field formulation is valid when the source-receiver range exceeds the square of the aperture divided by the wavelength.

The time-domain expression for the beamformed pressure $P_B(s,t)$ is obtained by taking the inverse Fourier transform of Eq. (2),

$$P_B(s,t) = 2\,\mathrm{Re}\left\{ \int_0^\infty P_B(s,f) e^{-i2\pi ft} df \right\} = 2\,\mathrm{Re}\{P_{B+}(s,t)\}, \quad (3)$$

where $\mathrm{Re}\{\cdot\}$ represents the real part. The complex beamformed pressure $P_{B+}(s,t)$ can then be approximated using the method of stationary phase[3,15–17] when $k_{rn}r_o \gg 1$, as given in Eq. (A6) in Appendix A. The stationary phase approximation for Eq. (3) simplifies to Eq. (A8) if the relative phase shifts between the different frequency components of the source spectrum are negligible, which occurs when $Q(f) = |Q(f)|$, such as in an impulsive or Gaussian signal. This is the simplifying approximation that limits the present formulation to the domain of transient signals, which is clearest for introducing the concepts. A more general formulation for continuous broadband noise is possible,[13] as noted in Sec. I. The complex beamformed pressure in Eq. (3) can then be approximated as

$$P_{B+}(s,t) \simeq \frac{4\pi i}{\sqrt{8\pi\rho(z_o)}} e^{-i\pi/4} \times \sum_n |Q(\tilde{f})| \tilde{u}_n(z_o) \tilde{u}_n(z) \frac{\tilde{B}(s-\tilde{s}_n)}{\sqrt{\tilde{k}_{rn}r_o}} F_n(\tilde{f}), \quad (4)$$

where $\tilde{f}$ is the frequency component within the source band that satisfies

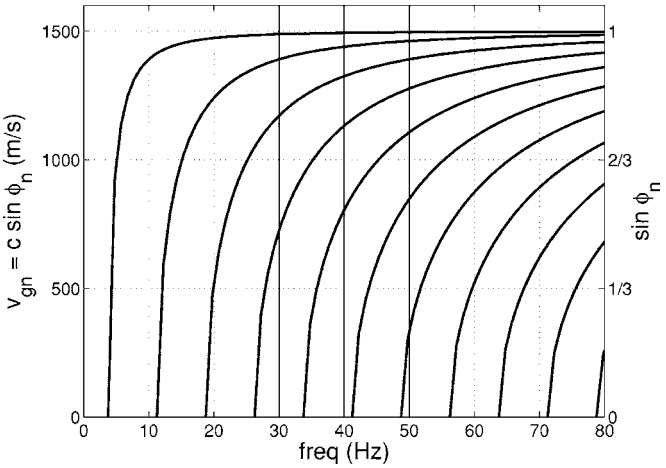

FIG. 3. Group velocity v_{gn} and modal elevation angle sin ϕ_n as a function of frequency in an ideal waveguide. The water depth and the sound speed are 100 m and 1500 m/s, respectively, and the boundaries are assumed to be pressure release. The vertical lines at 30, 40, and 50 Hz will be referred to in Fig. 5.

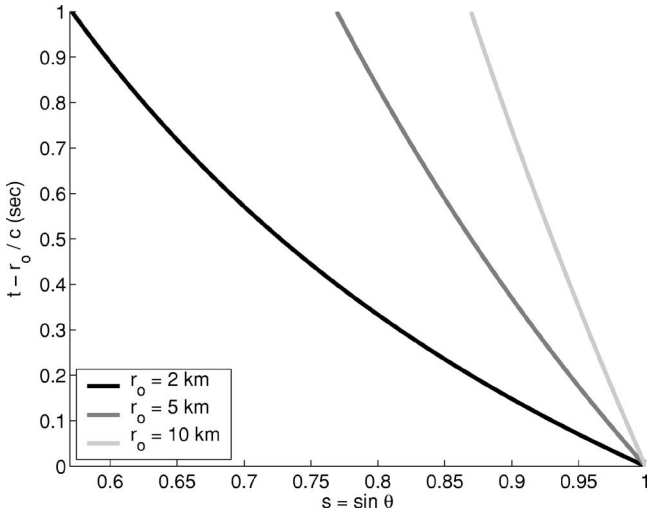

FIG. 4. The beam-time migration lines $\tilde{s}_n(t)$ as a function of reduced travel time $t-r_o/c$ and array scan angle θ for various source ranges over the full 0 to 80-Hz frequency band shown in Fig. 3. The sound speed c is 1500 m/s and source bearing θ_o is $\pi/2$. It can be seen that all the $\tilde{s}_n(t)$ merge to a single beamformer migration line $\tilde{s}(t)$.

$$t = \frac{r_o}{v_{gn}(\tilde{f})}, \tag{5}$$

v_{gn} is the group velocity of the nth mode, and $\tilde{u}_n, \tilde{k}_{rn}, \tilde{B}, \tilde{s}_n, \tilde{v}_{gn}, \tilde{\phi}_n$ are the corresponding values of $u_n, k_{rn}, B, s_n, v_{gn}, \phi_n$ at $f=\tilde{f}$. The function $F_n(\tilde{f})$ in Eq. (4) is given in Eq. (A9) of Appendix A. The bearing of peak beamformed pressure for the nth mode at time t is specified by

$$\tilde{s}_n(t) = \sin \tilde{\phi}_n(t) \sin \theta_o, \tag{6}$$

which is the zero of the argument of the beam pattern $\tilde{B}(s-\tilde{s}_n)$ in Eq. (4). Equations (5) and (6) enable the temporal migration of the maximum beamformer output angle to be determined in any horizontally stratified ocean waveguide. These equations are significant because they lead directly to source localization in an ocean waveguide by the new array invariant method.

B. Array invariant for horizontal arrays in ideal waveguides

Here we show that the bearing of peak beamformed pressure $\tilde{s}_n(t)$, given in Eq. (6) for any given mode at any time, is an observable from which source range can be estimated. This is done by first noting that group velocity and modal elevation angle are related by

$$[v_{gn}]^{-1} = \frac{1}{2\pi}\frac{d}{df}\sqrt{k^2 - k_{zn}^2} = \frac{1}{2\pi}\frac{dk}{df}\frac{k}{k_{rn}} = [c \sin \phi_n]^{-1} \tag{7}$$

for an ideal isovelocity waveguide with pressure-release or rigid boundaries since the vertical wavenumber of the nth mode k_{zn} is not a function of f. This is illustrated in Fig. 3. Then Eqs. (5) and (7) can be used to express Eq. (6) as

$$\tilde{s}_n(t) \equiv \tilde{s}(t) = \frac{r_o}{ct} \sin \theta_o, \tag{8}$$

which shows that the $\tilde{s}_n(t)$ merge to a single beamformer migration line $\tilde{s}(t)$ for all mode numbers if the source bandwidth is sufficiently large. For fixed source bearing, the beamformer migration line changes only as a function of source range as can be seen in Eq. (8) and as illustrated in Fig. 4.

If the bandwidth of the source signal is not sufficiently large, $\tilde{s}_n(t)$ may appear as discrete line segments along the trajectory described by the right-hand side of Eq. (8). This is due to the discrete nature of the waveguide modes. An example is shown in Fig. 5(a) for a source signal in the 30 to 40-Hz band. For a given frequency band, the length of an $\tilde{s}_n(t)$ segment is greater for higher-order modes. This is because they exhibit more dispersion than lower-order modes, as can be deduced from Fig. 3 by noting that the change in group velocity across the band increases with mode number.

For a given mode and $\tilde{s}_n(t)$ segment, the $\tilde{s}_n(t)$ will migrate to a different part of the $\tilde{s}(t)$ curve when the frequency band of the source signal changes. This is because both the group velocity and elevation angle of the given mode change as a function of frequency. This is illustrated in Fig. 5(b), where the source frequency is now in the 40 to 50-Hz band. Comparison of Figs. 5(a) and 5(b) shows that the $\tilde{s}_n(t)$ for a given mode migrates to an earlier segment with greater scan angle because both group velocity v_{gn} and elevation angle ϕ_n for that mode have increased with the positive shift in the bandwidth. This migration is constrained to occur within the $\tilde{s}(t)$ curve given by Eq. (8), which completely determines the peak beam-time migration in an ideal waveguide. If the source signal occupies the entire 30 to 50-Hz band, the $\tilde{s}_n(t)$ for individual modes overlap to form the continuous $\tilde{s}(t)$, as shown in Fig. 5(c).

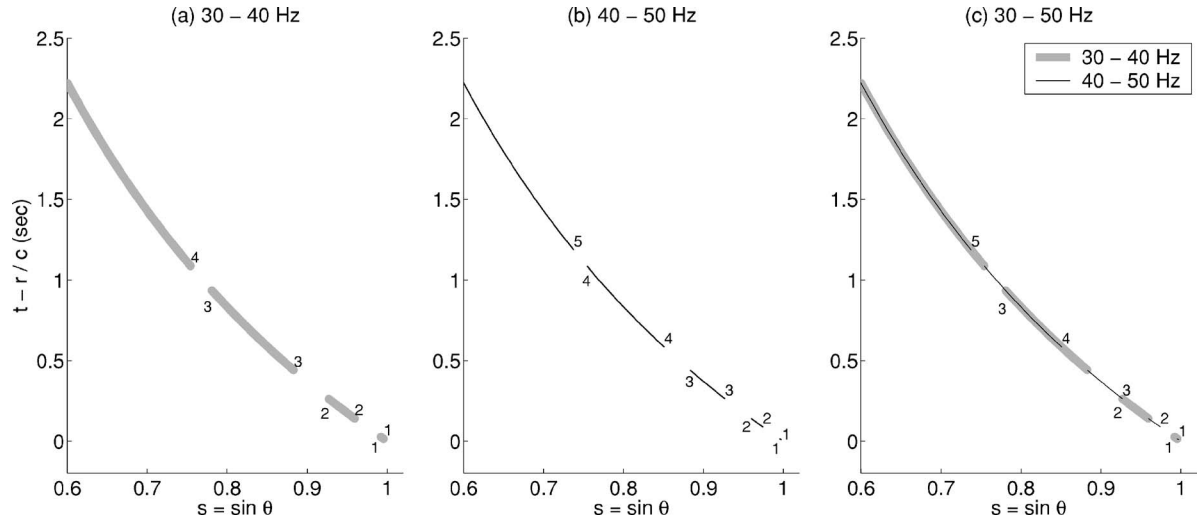

FIG. 5. (a) The beam-time migration lines $\tilde{s}_n(t)$ for modes in the 30 to 40-Hz band shown in Fig. 3 as a function of reduced travel time $t-r_o/c$ and array scan angle θ for a source at $r_o=5$ km and $\theta_o=\pi/2$. The beam-time migration lines $\tilde{s}_n(t)$ appear as discrete line segments. The beginning and end of each $\tilde{s}_n(t)$ segment is marked by mode number n. (b) The same as (a), but for modes in the 40 to 50-Hz band. As group velocity and elevation angle of a given mode changes, $\tilde{s}_n(t)$ for that mode migrates to a different location in the beam-time plot. This migration is constrained to occur within the $\tilde{s}(t)$ curve given by Eq. (8). (c) The same as (a), but for modes in the 30 to 50-Hz band. As the frequency band of the source increases, $\tilde{s}_n(t)$ for the individual modes overlap to form the continuous $\tilde{s}(t)$.

We define an array invariant χ_h for a horizontal linear receiver array as

$$\chi_h \equiv \frac{d\tilde{s}^{-1}(t)}{dt} = \frac{c}{r_o \sin\theta_o}. \tag{9}$$

For fixed source bearing, Eq. (9) is independent of source frequency band, mode number, source depth, receiver depth, and waveguide depth. Also, Eq. (9) is valid for both pressure release and rigid boundary ideal waveguides.

Source range can now be estimated using

$$\hat{r}_o = \frac{c}{\hat{\chi}_h \sin\hat{\theta}_o}, \tag{10}$$

based on direct measurements of the array invariant $\hat{\chi}_h$ and source bearing $\hat{\theta}_o$ obtained from beam-time intensity data. Since Eq. (10) is a unique one-to-one mapping of $\hat{r}_o$ from $\hat{\chi}_h$ for fixed $\hat{\theta}_o$, range inversion using the array invariant does not suffer from ambiguity, as is common in MFP.

The array invariant method differs significantly from the waveguide invariant method in that the array invariant does not rely on modal interference. Application of the waveguide invariant is not possible, for example, if there is only one mode propagating in a waveguide. The array invariant, however, is still applicable if the solitary mode causes sufficient dispersion in the source band, as can be seen in Eq. (8) and Fig. 4. In most practical applications, the combined dispersion of multiple modes is needed for robust source localization as will be shown in Sec. III.

C. Array invariant for horizontal arrays in stratified waveguides

For general horizontally stratified waveguides, the relationship between group velocity and horizontal wavenumber is

$$[v_{gn}]^{-1} = \frac{1}{2\pi}\frac{d}{df}\sqrt{k^2(z)-k_{zn}^2(z)},$$

which leads to the relation

$$v_{gn} = \frac{c(z)\sin\phi_n(z)}{1+\dfrac{c(z)}{2\pi}\cos\phi_n(z)\dfrac{dk_{zn}(z)}{df}} \tag{11}$$

between group velocity and modal elevation angle. By substituting Eq. (11) into Eq. (6), the peak beam-time migration line $\tilde{s}_n(t)$ for a given mode can be written explicitly as

$$\begin{aligned}\tilde{s}_n(z,t) &= \sin\tilde{\phi}_n(z,t)\sin\theta_o \\ &= \frac{r_o}{c(z)t}\sin\theta_o\left\{1+\frac{c(z)}{2\pi}\cos\tilde{\phi}_n(z)\left[\frac{dk_{zn}(z)}{df}\right]_{f=\tilde{f}}\right\}.\end{aligned} \tag{12}$$

The second term in the bracket in Eq. (12) is the correction term for the beamformer migration when there is variation in sound speed structure versus depth. This correction term for the nth mode is negligible when

$$\left|\frac{1}{2\pi}\left[\frac{dk_{zn}(z)}{df}\right]_{f=\tilde{f}}\right| \ll |c(z)\cos\tilde{\phi}_n(z)|^{-1}, \tag{13}$$

as can be seen in Eq. (12). It will be shown in Sec. III that most of the modes propagating in shallow-water waveguides satisfy Eq. (13), since change of the vertical wavenumber

versus frequency is typically negligible for frequencies not near modal cut-off. We refer to modes that do not satisfy Eq. (13) as waterborne modes. This terminology for waterborne modes is similar to that used by Ref. 18. While Eq. (13) is not satisfied near modal cut-off frequencies, modal contributions near cut-off are negligible since the corresponding modal amplitudes decay rapidly as r_o increases.[19]

Equation (12) is then independent of mode number, and can be approximated as

$$\tilde{s}(z,t) \simeq \frac{r_o}{c(z)t} \sin\theta_o, \tag{14}$$

where the departure from Eq. (8) is that sound speed at the receiver depends on receiver depth.

An array invariant for a general horizontally stratified waveguide is then defined as

$$\chi_h \equiv \frac{d\tilde{s}^{-1}(z,t)}{dt} \simeq \frac{c(z)}{r_o \sin\theta_o}, \tag{15}$$

where source range can again be estimated from Eq. (10) but with $c(z)$ substituted for c. The sound speed dependence of Eq. (15) is not an impediment since the sound speed at receiver depth can be readily measured by expendable bathythermographs (XBT). If such measurements are not available, $c(z)=1490$ m/s can be used for range estimation, which leads to only 3% error for the typical range of sound speeds, roughly 1440 to 1540 m/s, encountered in continental shelf waveguides.[20]

An array invariant can also be defined in another way. In practical shallow-water waveguides, the maximum extent of the exact beam-time migration line $\tilde{s}_n(z,t)$ along the beam-time migration line for non-waterborne modes $\tilde{s}(z,t)$ is limited by the time of the latest modal arrival, which is bounded by the minimum group velocity at the Airy phase. This maximum extent is typically sufficiently small that $d\tilde{s}(z,t)/dt$ can be expanded around $t=r_o/c(z)$, and only the zeroth-order term

$$\chi_l \equiv \frac{d\tilde{s}(z,t)}{dt} \simeq -\frac{c(z)}{r_o} \sin\theta_o \tag{16}$$

need be retained. Equation (16) defines an array invariant χ_l that is more convenient for practical use, and is a good approximation unless the seafloor is impenetrable. It will be used for source range estimation in Secs. III and IV.

D. Array invariant for vertical arrays in stratified waveguides

The array invariant method can also be used to instantaneously estimate source range from vertical line array measurements. The sound speed across the aperture of the array is taken to be approximately constant. The geometry is shown in Fig. 1(b). The beamformed pressure of the vertical array as a function of array scan angle ϕ is

$$P_{B,v}(s_v,f) = 4\pi Q(f) \frac{i}{\sqrt{8\pi}\rho(z_o)} e^{-i\pi/4} \sum_n u_n(z_o) \frac{e^{ik_{rn}r_o}}{\sqrt{k_{rn}r_o}} \times [N_n^+ B(s_v - s_{v,n}) + N_n^- B(s_v + s_{v,n})], \tag{17}$$

where $s_v=\cos\phi$, $s_{v,n}=\cos\phi_n$. Here, N_n^+ and N_n^- are the plane-wave amplitudes of the nth mode that satisfy $u_n(z) = N_n^+ e^{ik_{zn}z} + N_n^- e^{-ik_{zn}z}$ at the receiver depths z spanned by the array. For evanescent modes, $s_{v,n}$ does not lie in real space since $\cos\phi_n = i\sinh\phi_n'$. The time-domain complex beamformed pressure is approximated as

$$\tilde{P}_{B,v+}(s_v,t) \simeq \frac{4\pi i}{\sqrt{8\pi}\rho(z_o)} e^{-i\pi/4} \sum_n |Q(\tilde{f})| \tilde{u}_n(z_o) \frac{e^{i\tilde{k}_{rn}r_o}}{\sqrt{\tilde{k}_{rn}r_o}} \times [\tilde{N}_n^+ \tilde{B}(s_v - \tilde{s}_{v,n}) + \tilde{N}_n^- \tilde{B}(s_v + \tilde{s}_{v,n})] F_n(\tilde{f})$$

by the stationary phase method, where $\tilde{N}_n^+, \tilde{N}_n^-, \tilde{s}_{v,n}$ are the corresponding values of $N_n^+, N_n^-, s_{v,n}$ at the frequencies $\tilde{f}$ that satisfy Eq. (5).

For an ideal waveguide, group velocity and elevation angle are related by $v_{gn}=c\sqrt{1-\cos^2\phi_n}$, which can be obtained from Eq. (7). The beam-time migration line for a vertical array in an ideal waveguide then obeys

$$\pm\tilde{s}_{v,n}(t) \equiv \pm\tilde{s}_v(t) = \pm\sqrt{1-\left(\frac{r_o}{ct}\right)^2}, \tag{18}$$

and the migration lines $\tilde{s}_{v,n}(t)$ for all the modes merge to a single line $\tilde{s}_v(t)$. The signs specify whether the migration is vertically up or down. This is due to the symmetry of up and down-going plane-wave components of the modes when the sound speed across the array aperture is constant.

An array invariant χ_v for vertical arrays can be defined as

$$\chi_v \equiv \frac{d}{dt}[1-\tilde{s}_v^2(t)]^{-1/2} = \frac{c}{r_o}, \tag{19}$$

using Eq. (18). Source range can then be estimated as $\hat{r}_o = c/\hat{\chi}_v$, after measuring $\hat{\chi}_v$ from the migration of $\tilde{s}_v(t)$ in the given beam-time intensity data set. Linearization of $d\tilde{s}_v(t)/dt$ using a Taylor series expansion is not appropriate for vertical arrays since the zeroth-order term of $d\tilde{s}_v(t)/dt$ at $t=r_o/c$ is not finite.

The array invariant approach for vertical arrays can be applied in a general horizontally stratified waveguide when the sound speed $c(z)$ is constant across the aperture of the array. Using Eq. (11) and relation (13), the beam-time migration line in this scenario is

$$\pm\tilde{s}_{v,n}(z,t) \equiv \pm\tilde{s}_v(z,t) \simeq \pm\sqrt{1-\left(\frac{r_o}{c(z)t}\right)^2}, \tag{20}$$

from which the array invariant becomes

$$\chi_v \equiv \frac{d}{dt}[1-\tilde{s}_v^2(z,t)]^{-1/2} \simeq \frac{c(z)}{r_o}, \tag{21}$$

so that source range can be estimated as $\hat{r}_o = c(z)/\hat{\chi}_v$.

Equations (20) and (21) are also good approximations if the sound speed is not constant along the array aperture in

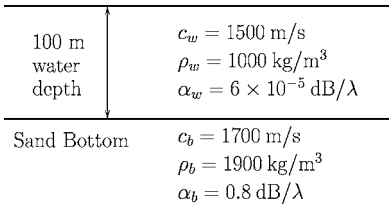

FIG. 6. The Pekeris waveguide with sand bottom, where c_w, ρ_w, and α_w are the sound speed, density, and attenuation of the water column, and c_b, ρ_b, and α_b are those of the sea-bottom.

general horizontally stratified waveguides so long as the variation of $k_{zn}(z)$ along the aperture of an array satisfies

$$|k_{zn}(z)(z-z_c) - k_{zn}(z_c)(z-z_c)| < \frac{\pi}{4}, \tag{22}$$

where z_c is the center depth of an array. The worst case would then occur at either end of the array for waves propagating parallel to the z-axis. Equation (22), with the approximation $1/c(z) = 1/(c(z_c)+\Delta c(z)) \simeq c^{-1}(z_c)(1-\Delta c(z)/c(z_c))$ where $\Delta c(z)$ is the sound speed difference at z_c and depths z spanned by the array, leads to a more practical condition

$$|\Delta c(z)| < \frac{c(z_c)}{2L/(\lambda(z_c)/2)} \tag{23}$$

for the sound speed variation along the array aperture for source range estimation using Eq. (21), where $\lambda(z_c) = k(z_c)/2\pi$ and L is the array aperture. For a typical vertical array aperture of $L = 64\lambda(z_c)/2$ and $c(z_c) = 1490$ m/s, Eq. (23) requires that the relatively benign condition $|\Delta c(z)| < 11$ m/s must be satisfied for Eqs. (20) and (21) to be good approximations.

III. ILLUSTRATIVE EXAMPLES BY SIMULATION

A. Horizontal array

Instantaneous source range estimation by the array invariant method is illustrated by a number of examples involving typical continental shelf environments and array configurations. The first example employs a horizontal receiving array in a Pekeris waveguide. The environmental parameters are shown in Fig. 6. The detection geometry is defined by $z = 30$ m, $z_o = 50$ m, $r_o = 5$ km, and $\theta_o = 60°$. The source signal is impulsive in the time-domain and bandlimited to 390 to 440 Hz by a Tukey filter.[21] The source level is 219 dB *re* 1 μPa at 1 m. The array aperture L is 94.5 m, and is tapered by a Hann window. The source, receiver, and geoacoustic parameters of the seabed are chosen for consistency with the field experiment described in Sec. IV.

The acoustic field from the impulsive source is measured as a time-series on each hydrophone sensor of the horizontal array. The hydrophone time-series data are converted to beam-time data by standard time-domain beamforming. Only the beam-time sound pressure level $L_{\text{bt}}(s,t) = 20\log|P_B(s,t)/1\ \mu\text{Pa}|$, which forms a two-dimensional image as shown in Fig. 7(a), is necessary for range estimation by the array invariant method.

The source range estimate

$$\hat{r}_o = -\frac{c(z)}{\hat{\chi}_l}\sin\hat{\theta}_o \tag{24}$$

is then a function of the estimates $\hat{\theta}_o$ and $\hat{\chi}_l$ based on the $L_{\text{bt}}(s,t)$ data. As noted in Sec. II C, the assumption $c(z) = 1490$ m/s is employed if no local sound speed measurements are available.

The source bearing estimate $\hat{\theta}_o$ is taken as the scan angle that corresponds to the global maximum of the beam-time sound pressure level data $L_{\text{bt}}(s,t)$. This is typically a good approximation in any continental shelf environment because (1) the global maximum is dominated by contributions from the earliest arrivals corresponding to the lowest-order modes, which typically suffer the least attenuation and dispersion, and (2) these modes typically satisfy $\sin\phi_n \simeq 1$ so that the global maximum occurs at $\sin\phi_n \sin\theta_o \simeq \sin\theta_o$, as can be seen from Eq. (6). The location of the global maximum is found by an automated exhaustive search through the $L_{\text{bt}}(s,t)$ data, leading to the estimate $\hat{\theta}_o = 59.8°$, which is consistent with the value obtained by inspection of Fig. 7(a), and is within a fraction of a degree of the true bearing.

The array invariant χ_l is estimated from the data by first finding

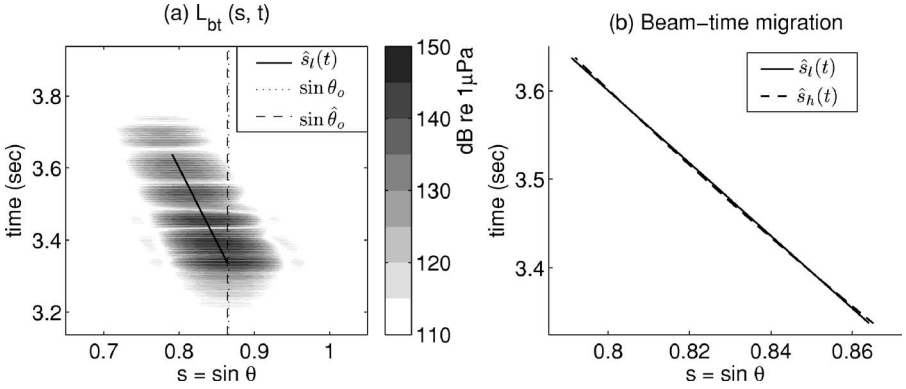

FIG. 7. (a) Beam-time image $L_{\text{bt}}(s,t)$ with true source range $r_o = 5$ km and bearing $\theta_o = 60°$ in the Pekeris sand waveguide. The dotted and dashed vertical lines are at $\sin\theta_o$ and $\sin\theta_o$, respectively, where $\hat{\theta}_o$ is the scan angle of the array corresponding to the global maximum of the $L_{\text{bt}}(s,t)$ data. The black solid line is the linear least squares fit $\hat{s}_l(t)$ of peak intensity angle versus time using Eq. (26). (b) The black solid line is the same $\hat{s}_l(t)$ as shown in (a), and the black dashed line is the linear least squares fit $\hat{s}_h(t)$ using Eq. (28). The two least squares fits are nearly identical to each other.

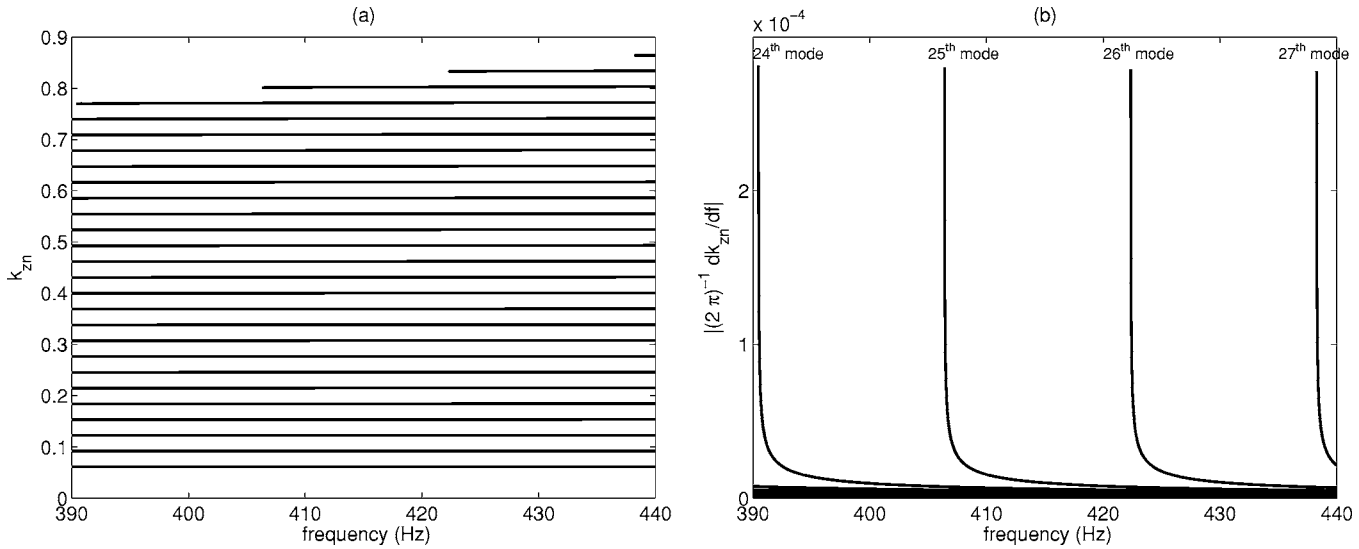

FIG. 8. (a) Vertical wavenumber k_{zn} versus frequency for modes in the Pekeris sand waveguide of Fig. 6. Each horizontal line corresponds to a specific mode. Higher-order modes have higher wavenumbers. (b) Frequency derivatives of k_{zn}. This figure shows that k_{zn} is effectively a constant function of frequency so that relation (13) is satisfied for the Pekeris waveguide except near mode cut-off.

$$s_{\max}(t) = \arg\max_{s} L_{\mathrm{bt}}(s,t)$$

by an automated peak detection algorithm. A least squares estimate of $\hat{\chi}_l$ is then found under the linear approximation

$$\hat{s}_l(t) = \hat{\chi}_l t + d_l \tag{25}$$

from Eq. (16), where d_l is a constant intercept. By this approach, the array invariant estimate $\hat{\chi}_l$ would explicitly be the first element of the vector

$$[\hat{\chi}_l \quad d_l]^T = (\mathbf{T}^T\mathbf{T})^{-1}\mathbf{T}^T\mathbf{S_1}, \tag{26}$$

where $\mathbf{S_1}=[s_{\max}(t_1), s_{\max}(t_2), \cdots, s_{\max}(t_N)]^T$, $\mathbf{T}=[(t_1, t_2, \cdots, t_N)^T\mathbf{1}^T]$, $t_j=t_1+(j-1)\Delta t_s$, Δt_s is the sample spacing in time, and $\mathbf{1}$ is an $1\times N$ matrix given by $\mathbf{1}=[1, 1, \cdots, 1]$. Other methods of estimation could be used such as the maximum likelihood or the Radon transform method. If the received field undergoes circular complex Gaussian fluctuations due to transmission through a random waveguide, or due to a random source, the least squares estimate of the log transformed beam-time intensity data is approximately the maximum likelihood estimator.[22,23]

The linear least squares fit $\hat{s}_l(t)$ of Eq. (25) is overlain on the $L_{\mathrm{bt}}(s,t)$ data in Fig. 7(a). The slope of the fitted line is the array invariant estimate, $\hat{\chi}_l=-0.244$. The corresponding source range estimate is then $\hat{r}_o \simeq 5.3$ km, from Eq. (24), which is within 6% of the true range $r_o=5$ km.

A slightly more accurate source range estimate can be obtained from

$$\hat{r}_o = \frac{c(z)}{\hat{\chi}_h \sin\hat{\theta}_o}, \tag{27}$$

where a least squares estimate of $\hat{\chi}_h$ is found under the approximation $\hat{s}_h^{-1}(t)=\hat{\chi}_h t+d_h$ from Eq. (15), with

$$[\hat{\chi}_h \quad d_h]^T = (\mathbf{T}^T\mathbf{T})^{-1}\mathbf{T}^T\mathbf{S_h}, \tag{28}$$

$\mathbf{S_h}=[s_{\max}^{-1}(t_1), s_{\max}^{-1}(t_2), \cdots, s_{\max}^{-1}(t_N)]^T$, and d_h as a constant intercept. The resulting least squares fit is shown in Fig. 7(b), where $\hat{\chi}_h=0.355$. The estimate of source range is then $\hat{r}_o \simeq 4.9$ km, from Eq. (27), which is within 2% of the true range.

In these examples, we do not use knowledge of the environment to estimate source range. This is necessary to show that the array invariant method can be used for range estimation simply by use of Eqs. (24), (27), and incoherent beam-time data $L_{\mathrm{bt}}(s,t)$.

The array invariant method works because relation (13) is satisfied in the given Pekeris waveguide environment as can be seen in Fig. 8, where the vertical wavenumber of the 27 propagating modes and their frequency derivatives are plotted. The vertical wavenumbers are nearly constant except near modal cutoff frequencies. Relation (13) is then satisfied for all modes except near cutoff, as can be seen in Fig. 8(b). The components near cutoff, however, do not contribute to the acoustic pressure as noted in Sec. II C, and can be neglected.

The array invariant method also works because the exact beam-time migration line $\tilde{s}_n(z,t)$ is well approximated by the least squares fits. The exact beam-time migration line $\tilde{s}_n(z,t)$, calculated using Eq. (12), is shown in Fig. 9(a) as a black line. The temporal extent of $\tilde{s}_n(z,t)$ is limited by the time of the latest modal arrival in the source band, as discussed in Sec. II C. The detailed shape of $\tilde{s}_n(z,t)$ is plotted in Fig. 9(b), which shows that $\tilde{s}_n(z,t)$ can be well approximated by the least squares fits given in Eqs. (26) and (28).

B. Vertical array

Here we show that source range can be instantaneously estimated using the array invariant for vertical arrays with a

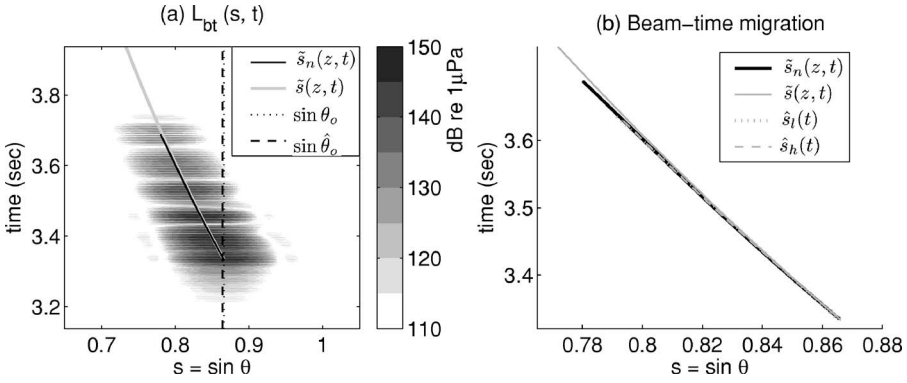

FIG. 9. (a) Beam-time image $L_{\mathrm{bt}}(s,t)$ identical to that in Fig. 7. The black solid line is the exact beam-time migration line $\tilde{s}_n(z,t)$ given in Eq. (12), for modes up to $n=23$. The last four modes with mode cut-off in the 390 to 440-Hz band, as shown in Fig. 8, are neglected. The gray solid line is the beam-time migration line for non-waterborne modes $\tilde{s}(z,t)$ from Eq. (14). (b) The black and gray solid lines are the detailed shapes of the same $\tilde{s}_n(z,t)$ and $\tilde{s}(z,t)$ shown in (a). The two least squares fits $\hat{s}_l(t)$ and $\hat{s}_h(t)$ in Fig. 7, overlain as gray dashed and dotted lines, show good agreement with the exact beam-time migration line $\tilde{s}_n(z,t)$.

Pekeris waveguide example. The environmental parameters are shown in Fig. 6. The detection geometry is defined by $z_c=50$ m, $z_o=50$ m, and $r_o=5$ km. The source signal is impulsive in the time domain and bandlimited in 390 to 440 Hz by a Tukey filter. The source level is 219 dB *re* 1 μPa at 1 m. The array aperture L is 94.5 m, and is tapered by a Hann window.

The acoustic field from the impulsive source is measured as a time-series on each element of the vertical array. The time-series data are converted to beam-time data by standard time-domain beamforming. The beam-time sound pressure level $L_{\mathrm{bt}}(s_v,t)=20\log|P_B(s_v,t)/1\ \mu\mathrm{Pa}|$ is shown in Fig. 10(a). The $L_{\mathrm{bt}}(s_v,t)$ data are symmetric with respect to array broadside, where $s_v=0$, since each mode is composed of an up and a down-going plane wave component with equal amplitude in the water column. Only $L_{\mathrm{bt}}(s_v>0,t)$ is shown in Fig. 10(a). Resolution of lower-order modes is significantly better for the vertical array than the horizontal array since equivalent plane waves are incident near broadside in the former.[24]

Source range can be estimated from

$$\hat{r}_o=\frac{c(z)}{\hat{\chi}_v}, \tag{29}$$

where a least squares estimate of $\hat{\chi}_v$ is found with the approximation $[1-\hat{s}_v^2(t)]^{-1/2}=\hat{\chi}_v t+d_v$ from Eq. (21), by

$$[\hat{\chi}_v \quad d_v]^T=(\mathbf{T}^T\mathbf{T})^{-1}\mathbf{T}^T\mathbf{S}_\mathbf{v}, \tag{30}$$

where $\mathbf{S}_\mathbf{v}=[(1-s_{\max}^2(t_1))^{-1/2},(1-s_{\max}^2(t_2))^{-1/2},\cdots,(1-s_{\max}^2(t_N))^{-1/2}]^T$, and d_v is a constant intercept. Since the beam-time intensity is symmetric with respect to the $s_v=0$ axis, $s_{\max}(t)$ can be found either from

$$s_{\max}(t)=\arg\max_{s_v>0} L_{\mathrm{bt}}(s_v,t),$$

or from

$$s_{\max}(t)=\arg\max_{s_v<0} L_{\mathrm{bt}}(s_v,t).$$

The resulting least squares fit is overlain in Fig. 10(a) as a black line, where $\hat{\chi}_v=0.312$. The corresponding source

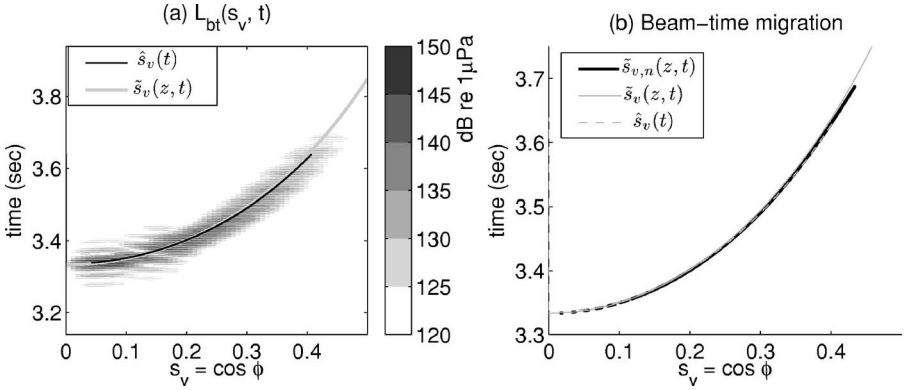

FIG. 10. (a) Beam-time image $L_{\mathrm{bt}}(s_v,t)$ for $r_o=5$ km in the Pekeris sand waveguide. The black solid line is the linear least squares fit $\hat{s}_v(t)$ of peak intensity versus time calculated using Eq. (30). The gray solid line is the beam-time migration line for non-waterborne modes, $\tilde{s}_v(z,t)$, in Eq. (18). (b) The black solid line is the exact beam-time migration line $\tilde{s}_{v,n}(z,t)$. The gray solid and dashed lines are $\tilde{s}_v(z,t)$ and $\hat{s}_v(t)$ in (a), respectively. It can be seen that the exact beam-time migration line $\tilde{s}_{v,n}(z,t)$ can be well approximated by the least squares fit $\hat{s}_v(t)$.

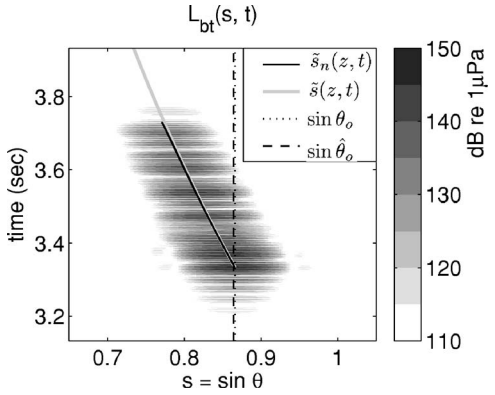

FIG. 11. The same as Fig. 9(a), but for the 150-m deep Pekeris sand waveguide. The exact beam-time migration line $\tilde{s}_n(z,t)$ is plotted for the first 36 modes of the 41 propagating modes. It can be seen by comparison of Fig. 9(a) and Fig. 11 that the exact beam-time migration line $\tilde{s}_n(z,t)$ in a Pekeris waveguide is invariant over the waveguide depth.

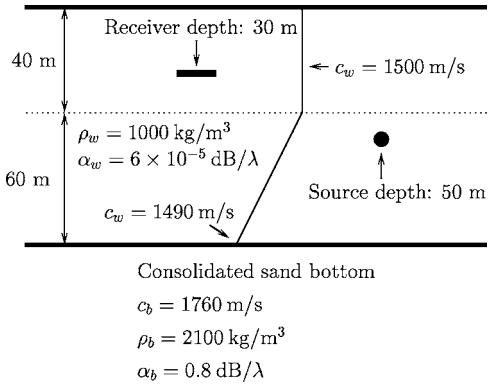

FIG. 12. Horizontally stratified waveguide with linear sound speed gradient. The sound speed is constant up to 40-m depth, and linearly decreases to 1490 m/s at 100-m depth. The density and attenuation of the water column are the same as those in Fig. 6, but the geoacoustic parameters of the sea-bottom are assumed to be different.

range estimate is then $\hat{r}_o \simeq 4.8$ km, from Eq. (29), which is within 4% of the true range $r_o = 5$ km.

C. Environmental invariance

Here we illustrate the environmental invariance of the range estimation equations (24) and (27) with some examples. We first note that the array invariants χ_l and χ_h are effectively identical for the 100-m deep Pekeris waveguide of Fig. 9, and for the 150-m deep Pekeris waveguide of Fig. 11. This is because the migration of $\tilde{s}_n(z,t)$ in response to the given change in waveguide depth occurs only within $\tilde{s}(z,t)$, as discussed in Sec. II. From this example, it can also be deduced that the same invariance holds over frequency. This is because the dispersion relation in a Pekeris waveguide with water depth H effectively depends only on the nondimensional parameter Hf/c_w for fixed ρ_b/ρ_w and c_b/c_w, as shown in Fig. 4–10 of Ref. 15.

The next example illustrates that array invariants are insensitive to the detailed sound speed profile of the water column and the geoacoustic parameters of the sea-bottom. Figure 12 shows an ocean waveguide with a sound speed gradient in the water column. The sound speed changes linearly from 1500 m/s at $z=40$ m to 1490 m/s at $z=100$ m. The sea-bottom is assumed to be a consolidated sand bottom with geoacoustic parameters given in Fig. 12. The true source range and bearing with respect to the receiver array are identical to those in Sec. III A.

The vast majority of modes satisfy relation (13), and the exact beam-time migration line $\tilde{s}_n(z,t)$ effectively span the entire $\tilde{s}(z,t)$ line shown in Fig. 13. Only the negligible portion of the line $\tilde{s}_n(z,t)$ at its temporal inception arises from waterborne modes that violate relation (13), as can be seen from Figs. 14 and 15. Source range can then be estimated following the same procedure in Sec. III A, by estimating $\hat{\chi}_l$ or $\hat{\chi}_h$ and using Eqs. (26) or (28).

IV. EXPERIMENTAL DEMONSTRATION OF THE ARRAY INVARIANT

We demonstrate the performance of the array invariant method at range estimation with field data acquired during the MAE of 2003 conducted in the New Jersey Strataform area. Water depth typically varied from 70 to 80 m, and source range from 1 to 8 km for the data considered.

A. Source, receiver geometry, and environmental parameters

The MAE was conducted in the New Jersey Strataform area to identify the causes of acoustic clutter in continental shelf environments.[25,26] Broadband source signals were

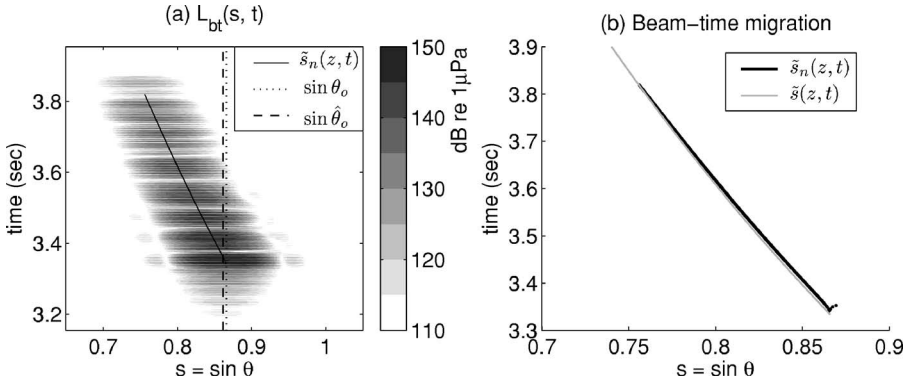

FIG. 13. Beam-time image $L_{bt}(s,t)$ for $r_o=5$ km and $\theta_o=60°$ in the environment shown in Fig. 12. The exact beam-time migration line $\tilde{s}_n(z,t)$ is plotted for the first 27 modes of the 31 propagating modes. The exact beam-time migration line $\tilde{s}_n(z,t)$ is nearly identical to that of the Pekeris waveguide shown in Fig. 9, and it effectively spans the entire $\tilde{s}(z,t)$ line.

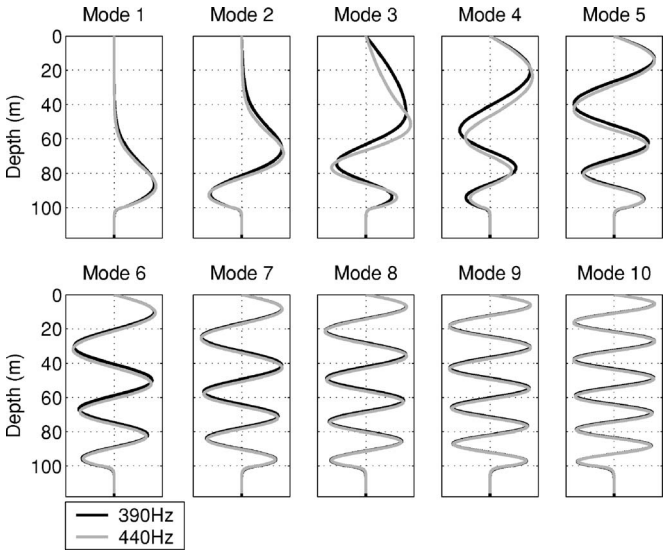

FIG. 14. Mode shape of the first ten modes at 390 and 440 Hz, for the environment shown in Fig. 12. Only the first three modes are waterborne since they are trapped in the refract-bottom-reflect sound speed channel between $z=40$ m and 100 m shown in Fig. 12.

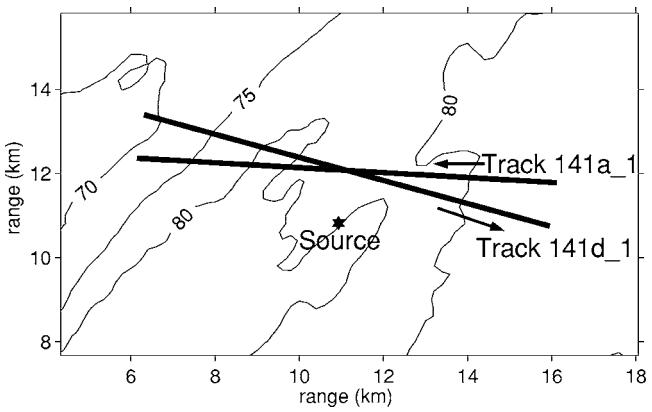

FIG. 16. The source position and the two receiver ship tracks on May 7, 2003. The source to receiver distance varied from 1 km to 6 km. The depth contour of the sea-bottom in meters is also shown in the figure. The arrows show the heading of the receiver ship along the tracks. The origin of the coordinates in Figs. 16 and 17 is at 38.955°N and 73.154°W.

transmitted from R/V Endeavor. A horizontal linear receiver array was towed along linear tracks by R/V Oceanus. The positions of the source and the tracks used in the present analysis are shown in Figs. 16 and 17. The positions of both research vessels were accurately measured by Global Positioning System (GPS).

Bathymetry is also plotted in Figs. 16 and 17. The seafloor has an extremely benign slope, typically less than 1°, as can be seen in Fig. 4 of Ref. 26. The seabed is mostly composed of sand with geoacoustic parameters given in Fig. 6.[25,26] Two or three XBTs were deployed per track from R/V Oceanus. The sound speed profiles measured by the XBTs are shown in Fig. 18.

The receiver was a horizontal line array with aperture $L=94.5$ m for the frequency band of the present analysis. Receiver array depth typically varied from 35 to 45 m for the tracks considered here. The source was a seven-element vertical line array with a 10-m aperture with center depth at 38.1 m. As will be shown later in this section, this vertical source array significantly suppressed the amplitudes of the higher-order modes by generating a narrow vertical beam of sound with roughly 6° 3-dB beamwidth. The source transmitted 1-second duration linear frequency modulated signals in the 390 to 440-Hz band every 50 seconds, roughly 100 transmissions per track.[25] The signal measured by the receiving array was tapered by a Hann window, beamformed, and then matched filtered with a replica signal. As shown in Appendix A, the array invariant derived for impulsive sources can also be applied to non-impulsive sources if the received field is phase conjugated by matched filtering. As noted in

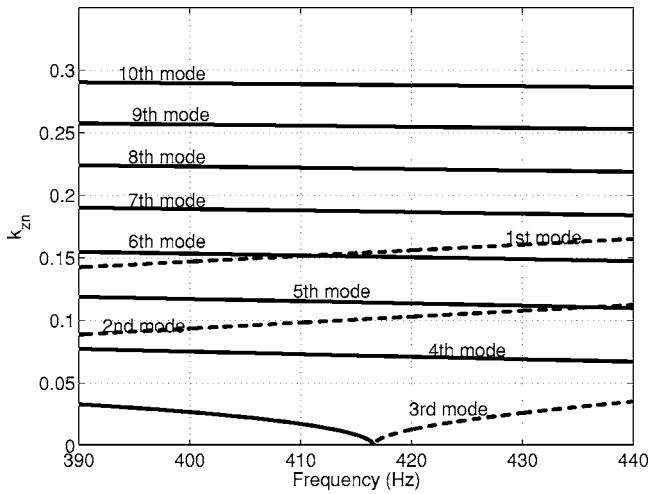

FIG. 15. Vertical wavenumber k_{zn} of the first ten modes in the environment shown in Im. 12. The solid lines represent Re$\{k_{zn}\}$, and the dashed lines represent Im$\{k_{zn}\}$. Only the first three modes are waterborne, and exhibit rapid change of k_{zn} versus frequency.

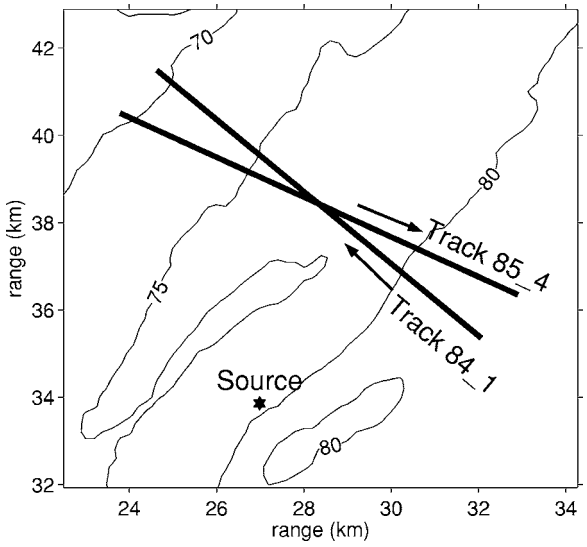

FIG. 17. The source position and the two receiver ship tracks on May 1, 2003. The source to receiver distance varied from 4 km to 8 km.

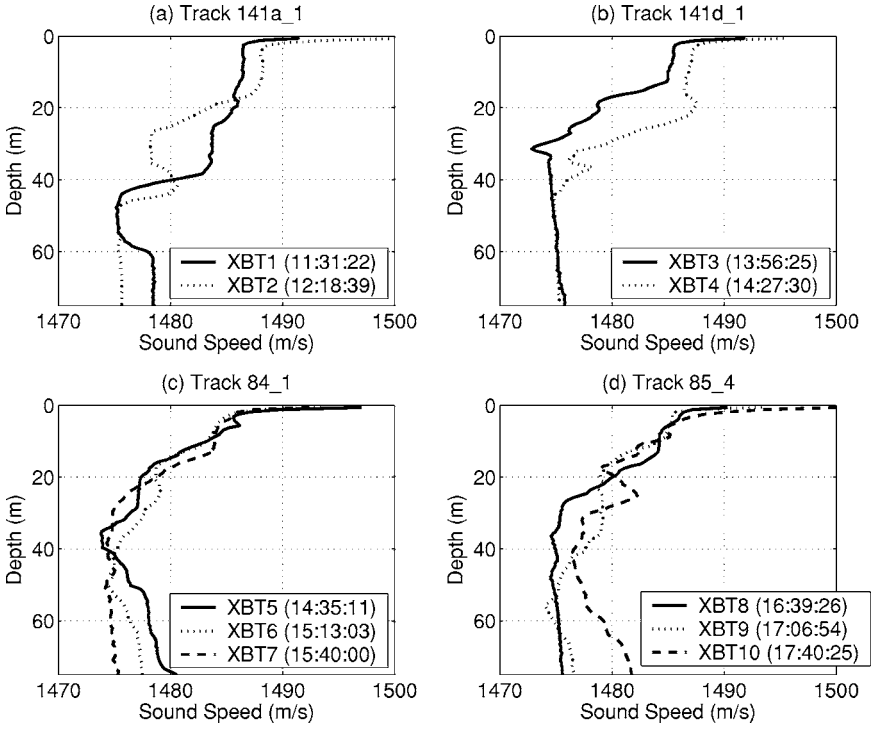

FIG. 18. Sound speed profiles measured by XBT's during the MAE 2003. Two XBTs were deployed for tracks 141a_1 and 141d_1 [(a) and (b)], and three XBTs were deployed for tracks 84_1 and 85_4 [(c) and (d)]. The Greenwich Mean Time of the deployment are shown in the parentheses.

Sec. I, a more general formulation that can treat arbitrary broadband signals that are not necessarily impulsive is possible.[13]

B. Instantaneous range estimation by the array invariant method

We show that source range can be instantaneously and accurately estimated using the array invariant method from field data. The measured beam-time sound pressure level data $L_{\mathrm{bt}}(s,t)$, obtained after time-domain beamforming and matched filtering of the acoustic field received on the horizontal array for a source transmission from Track 141d_1, is imaged in Fig. 19(a). The range and bearing of the source with respect to receiver coordinates are r_o=3.6 km and θ_o =−65° by GPS measurement. The linear least squares fit of the beam-time migration line $\hat{s}_l(t)$, calculated using Eq. (26), is overlain on Fig. 19(a). The slope of the fitted line is the array invariant estimate, $\hat{\chi}_l$=0.339. The source range r_o is then estimated as $\hat{r}_o=-c(z)\sin\hat{\theta}_o/\hat{\chi}_l\simeq 4.1$ km from Eq. (24). This is within 14% of the true range, which is sufficient for many practical applications.

A corresponding simulation is shown in Fig. 19(b). The simulated $\tilde{s}_n(z,t)$, overlain in Fig. 19(b), shows good agreement with the least squares fit of the beam-time migration line $\hat{s}_l(t)$ in Fig. 19(a). Figure 20 shows that vertical wavenumber is effectively a constant function of frequency so that relation (13) is satisfied for the MAE waveguide, which implies that the array invariant method should work well as shown in the example in Fig. 19.

We show that source range can be consistently and robustly estimated using the array invariant method with experimental field data. Source range was estimated 241 times for ranges between 1 and 8 km over a 6-hour period using MAE data. High correlation was found between source range

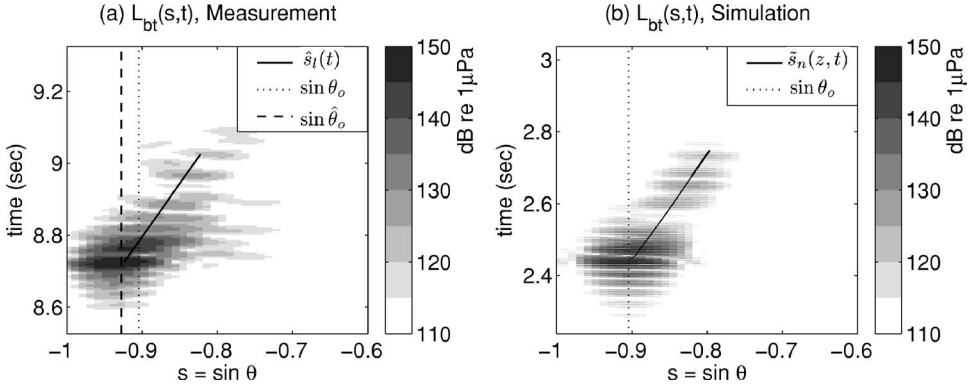

FIG. 19. (a) The beam-time sound pressure level image $L_{\mathrm{bt}}(s,t)$ measured during the MAE 2003. The dotted vertical line is at $\sin\theta_o$, and the dashed vertical line is at $\sin\hat{\theta}_o$, where θ_o=−65° and $\hat{\theta}_o$=−68°. The slanted line is the linear least squares fit of peak beam-time migration. The receiver depth is 39.7 m. (b) Simulation of the measurement shown in (a) using the sound speed profile in Fig. 18(b) XBT3. The positions of $\sin\theta_o$ and $\sin\hat{\theta}_o$ are nearly identical. The slant line is $\tilde{s}_n(z,t)$ up to the 20th mode.

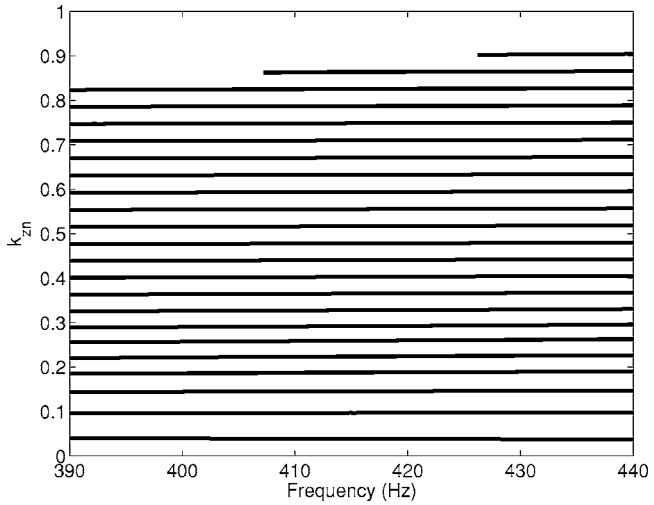

FIG. 20. Vertical wavenumbers k_{zn} at $z=39.7$ m calculated using the sound speed profile in Fig. 18(b) XBT3. This figure shows that relation (13) is satisfied for the MAE waveguide so that the array invariant method should be applicable. This is because the vertical wavenumber is effectively a constant function of frequency.

estimates using the array invariant method and ranges measured by GPS. The range estimates $\hat{r}_o$ using the array invariant method are shown in Fig. 21 along with the GPS measured ranges r_o for tracks 141a_1, 141d_1, 84_1, and 85_4. Only ping transmissions that have $20° < |\hat{\theta}_o| < 75°$ were used in range estimation since the array invariant for a horizontal array is insensitive to r_o at broadside incidence, and since the endfire resolution of a horizontal linear array is significantly worse than the near-broadside resolution.

Figure 22 shows range estimates $\hat{r}_o$ versus GPS measured ranges r_o for all four tracks. The solid line in Fig. 22 is the linear regression of $\hat{r}_o$ with respect to r_o. The regression coefficient and the correlation coefficient of 0.946 and 0.835, respectively, are high and indicate that the data have significantly supported the array invariant range estimation model.

The root mean square (rms) error of all range estimates determined by the array invariant method is 25% of the source range. The accuracy of this particular experimental configuration shows that the array invariant is of extreme practical value.

Even greater accuracy can be achieved for similar measurement scenarios if the source is omnidirectional. The vertical linear source array used in this experiment significantly degraded performance by suppressing higher-order modes, especially at long ranges. This is not typical of mobile sources that are detected and tracked in operational systems. Comparison of simulations in Fig. 9 and Fig. 19(b) shows that the amplitudes of the higher-order modes are significantly reduced by the beampattern of the source. This is especially noticeable since $r_o=5$ km in Fig. 9, whereas $r_o=3.6$ km in Fig. 19(b). This also appears in the experimental measurement in Fig. 19(a) where peak amplitude decays rapidly with increasing arrival time.

The length of the receiver array used in the MAE was roughly $64\lambda/2$, one-half the length of many standard arrays. Using a more typical $128\lambda/2$ aperture array would increase the range resolution by a factor of 2, since the range resolution of the array invariant method is roughly proportional to receiving array beamwidth.

Uncertainties in array position, tilt, and shape can also introduce range estimation error. Our numerical simulations show that a 1° tilt in both the horizontal and vertical, which was typical in the MAE,[25,26] can cause roughly a 10% error in the current source range estimates.

V. COMPARISON OF THE ARRAY INVARIANT METHOD TO OTHER RANGE ESTIMATION TECHNIQUES

It has been suggested that the interference pattern of incoherent acoustic intensity measured as a function of range and frequency can be used for source localization in shallow-water waveguides by the waveguide invariant method, provided that the values of the invariant parameters are known accurately.[9,10] The waveguide invariant parameter β_{mn} between two propagating modes m and n is defined as

$$\beta_{mn} = -\frac{v_{pm}^{-1} - v_{pn}^{-1}}{v_{gm}^{-1} - v_{gn}^{-1}}. \tag{31}$$

For an ideal waveguide with perfectly reflecting boundaries or for a waveguide with an n^2-linear sound speed profile, the waveguide invariant parameters are approximately equal to 1 and -3, respectively. Equation (31) shows that the waveguide invariant requires multiple modes in its fundamental definition, whereas the array invariant does not require multiple modes as discussed in Sec. II B.

Range estimation using the waveguide invariant can lead to large errors if the distribution of β_{mn} is not known *a priori* since uncertainty in r_o is proportional to uncertainly in β_{mn}. Incoherent intensity interference patterns measured during the MAE and corresponding waveguide invariant parameters are provided in Figs. 23 and 24, respectively, where it can be seen that β_{mn} can vary from 1 by more than a factor of 2. This variation of β_{mn} will lead to more than a factor of 2 error in range estimates if $\beta_{mn}=1$ is assumed without *a priori* knowledge of the waveguide invariant parameters. The waveguide invariant parameters also can suffer from large temporal and spatial variation. This is demonstrated in Fig. 24, where roughly a factor of 2 change in β_{mn} is shown to have occurred in less than 2 hours.

Range estimation using MFP techniques also requires accurate knowledge of the environmental parameters. For example, Fig. 9 in Ref. 7 shows that a very common uncertainty of only ±6 m/s sound speed mismatch in the water column results in intolerable MFP ambiguity in a 100-m deep shallow-water waveguide with a source at 5-km range.

The array invariant, waveguide invariant, and MFP techniques for passive source range estimation all fit into a similar category. This is because they all work even when the source is in the far-field of the receiver since they all rely on

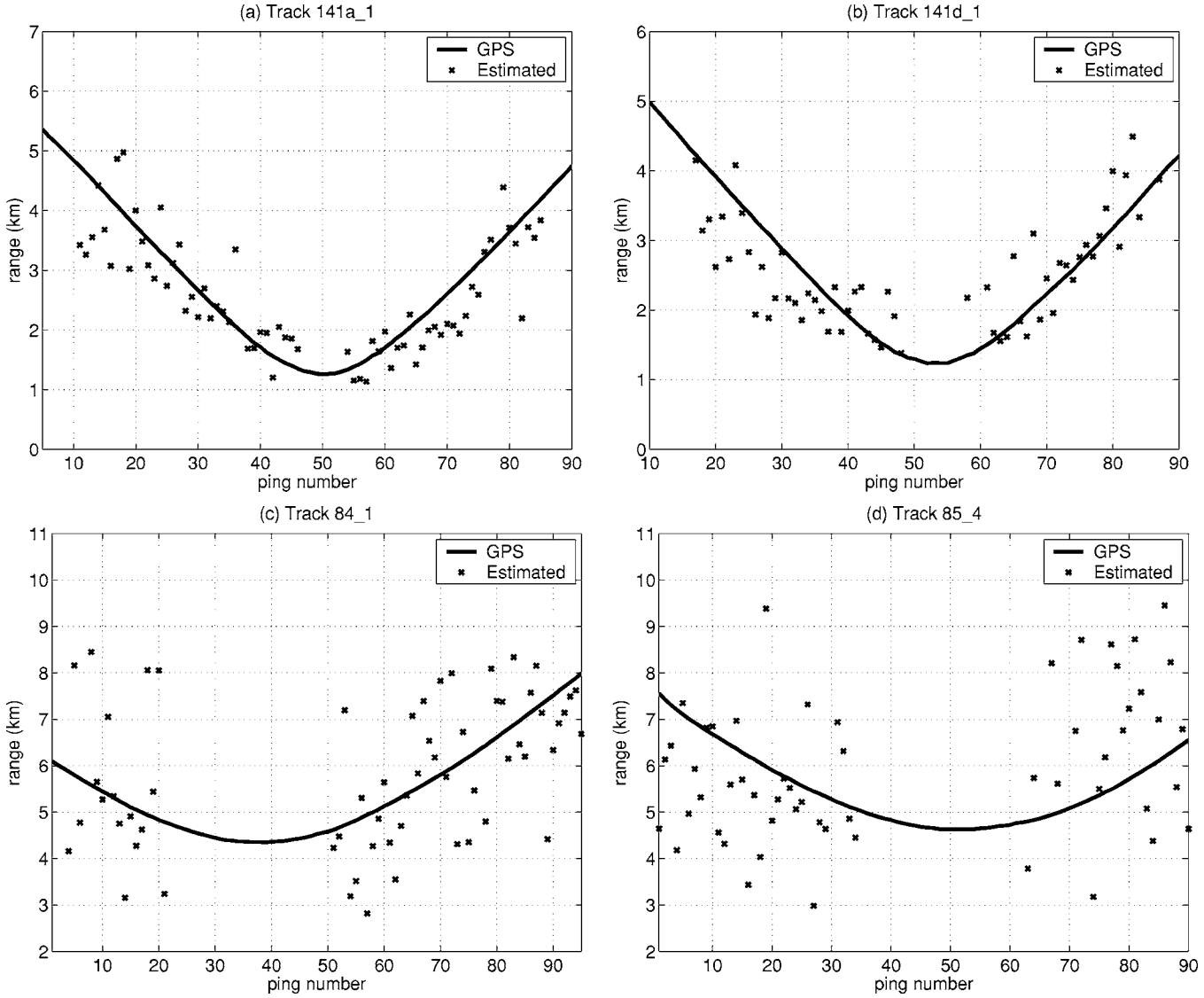

FIG. 21. Experimental range estimates using the array invariant method. The solid lines show r_o measured by GPS. The cross marks show $\hat{r}_o$ estimated by the array invariant method. (a) Track 141a_1: 66 range estimates are shown, and 3 noise-corrupted data are ignored. The rms error e_{rms} is 0.6 km. (b) Track 141d_1:58 range estimates are shown, and 4 noise-corrupted data is ignored. The rms error e_{rms} is 0.6 km. (c) Track 84_1: 61 range estimates are shown, and 8 noise-corrupted data are ignored. The rms error e_{rms} is 1.4 km. (d) Track 85_4: 56 range estimates are shown, and 6 noise-corrupted data are ignored. The rms error e_{rms} is 1.7 km.

the waveguide effects such as modal dispersion or interference. While near-field techniques for source localization, such as focusing or triangulation, may have better range resolution than any of these far-field waveguide techniques, they require an extended aperture or combination of widely separated apertures, which limits their practicality.

VI. CONCLUSION

The array invariant method has been introduced for instantaneous source range estimation in an ocean waveguide. The method exploits the dispersive behavior of guided wave propagation. It has been shown that the array invariant method does not require *a priori* knowledge of the environmental parameters, nor does it require extensive computations. The ability to make simple and accurate range estimates by the array invariant method has been demonstrated with data from the MAE of 2003.

APPENDIX A: STATIONARY PHASE APPROXIMATION APPLIED TO BEAMFORMING IN A WAVEGUIDE

The method of stationary phase has long been used in guided wave propagation problems to obtain the time-domain response at a receiver,[15,16] and to obtain the time-domain solution of the scattered field[3,17] by a broadband source. The stationary phase approximation used here is explicitly given in Appendix A 1, and applied to beamforming in a waveguide in Appendix A 2.

1. General stationary phase approximation

Let

$$I(x) = \int_a^b g(f) e^{ix\psi(f)} df, \tag{A1}$$

and let $\psi(f)$ satisfy $\psi^{(\nu)}(\tilde{f}) \neq 0$ and $\psi^{(1)}(\tilde{f}) = \psi^{(2)}(\tilde{f}) = \cdots = \psi^{(\nu-1)}(\tilde{f}) = 0$ at $f = \tilde{f}$, where $\psi^{(\nu)}(f)$ is the νth derivative of

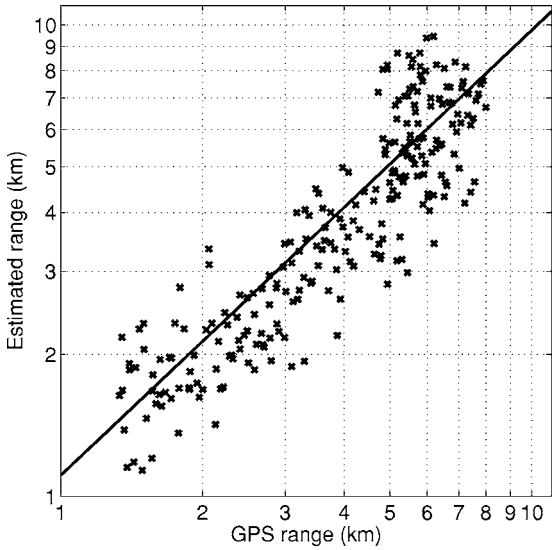

FIG. 22. Experimental range estimates using the array invariant method. The range estimates $\hat{r}_o$ versus GPS measured ranges r_o for tracks 141a_1, 141d_1, 84_1, and 85_4 plotted in logarithmic scale. The solid line is the linear regression $\hat{r}_o = a + br_o$, where the regression coefficient $b = 0.946$ and the intercept $a = 161$ m. The correlation coefficient is 0.835.

$\psi(f)$ with respect to f for positive integer ν. Then $\psi(f)$ can be expanded into the Taylor series as

$$\psi(f) \simeq \psi(\tilde{f}) + \frac{\psi^{(\nu)}(\tilde{f})}{\nu!}(f-\tilde{f})^{\nu}$$

near $f=\tilde{f}$, and Eq. (A1) can be approximated as

$$I(x) \simeq \begin{cases} 2g(\tilde{f})e^{ix\psi(\tilde{f})+\mathrm{sgn}(\psi^{(\nu)}(\tilde{f}))i\pi/2\nu}\left[\dfrac{\nu!}{x|\psi^{(\nu)}(\tilde{f})|}\right]^{1/\nu}\dfrac{\Gamma(1/\nu)}{\nu} & \text{if } \nu \text{ is even,} \\ 2g(\tilde{f})e^{ix\psi(\tilde{f})}\left[\dfrac{\nu!}{x|\psi^{(\nu)}(\tilde{f})|}\right]^{1/\nu}\dfrac{\Gamma(1/\nu)}{\nu}\cos\left(\dfrac{\pi}{2\nu}\right) & \text{if } \nu \text{ is odd,} \end{cases} \tag{A2}$$

for $x \gg 1$.[27] Solutions for the special cases of $\nu=2$ and $\nu=3$ can be found in Ref. 16. The error term introduced by the approximation in Eq. (A2) vanishes at a rate of $1/x$ and therefore is negligible for sufficiently large x.[27]

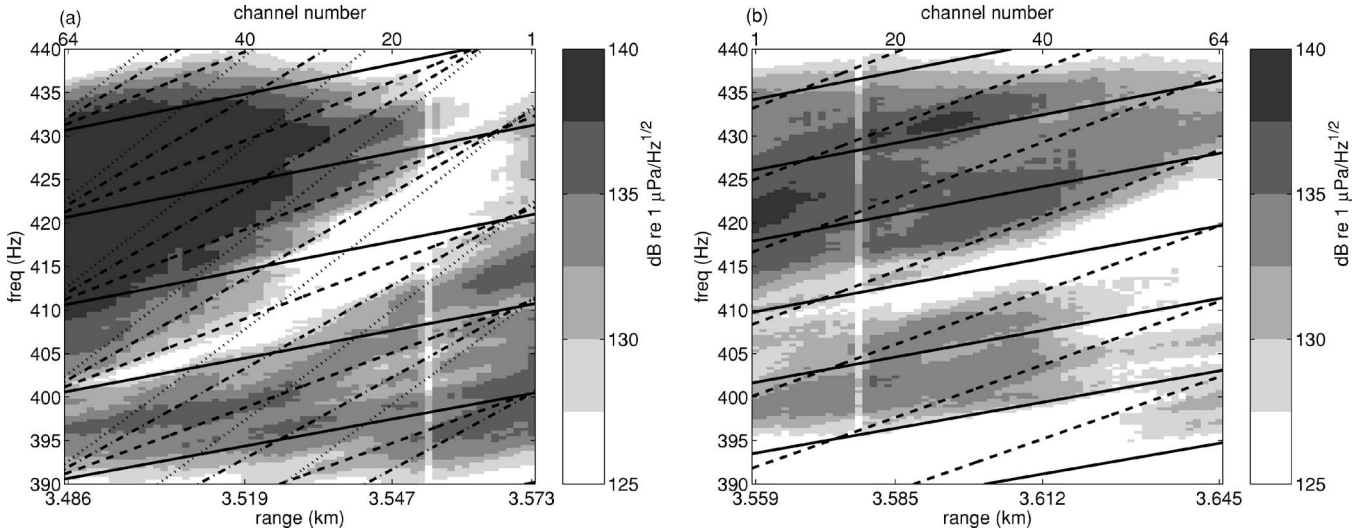

FIG. 23. Incoherent acoustic intensity measured over the array aperture during the MAE 2003. (a) is one of the measurements from Track 141a_1, and (b) is the incoherent intensity of the same data shown in Fig. 19 from Track 141d_1. The receiver array has 64 channels, the number of which are shown on top of the figures. The range from each channel to the source is shown at the bottom of the figures. The black lines are the interference patterns for $\beta_{mn}=1$ (—) $\beta_{mn}=2$ (---), $\beta_{mn}=3$ (-·--), and $\beta_{mn}=4$ (···), respectively, calculated using Eq. (31). Variation of β_{mn} from 1 by more than a factor of 2 can be observed.

2. Application of the stationary phase approximation for array beamforming

The complex beamformed pressure $P_{B+}(s,t)$ of Eq. (3) can be rewritten as

$$P_{B+}(s,t) = \frac{4\pi i}{\sqrt{8\pi\rho(z_o)}} e^{-i\pi/4} \sum_n \int_0^\infty |Q(f)| u_n(z_o) u_n(z) \times \frac{B(s-s_n)}{\sqrt{k_{rn} r_o}} e^{i r_o \psi_n(f)} df, \tag{A3}$$

where

$$\psi_n(f) = k_{rn} - \frac{2\pi f t - \angle Q(f)}{r_o}, \tag{A4}$$

and $|Q(f)|$ and $\angle Q(f)$ are the magnitude and phase of $Q(f)$. Then $\psi_n'(f)$ is zero at the frequency f that satisfies

$$t = \frac{r_o}{v_{gn}(\tilde{f})} + \frac{1}{2\pi} \frac{d}{df} \angle Q(f) \Big|_{f=\tilde{f}}, \tag{A5}$$

where $\tilde{f}$ is the dominant frequency component that arrives at the receiver array at time t. The first term in the right-hand side of Eq. (A5) is the travel time of the nth mode at $f=\tilde{f}$. The second term is the relative phase shift of the source spectrum, or the relative source time delay of the frequency component $\tilde{f}$. The stationary phase approximation of Eq. (A3) is then

$$P_{B+}(s,t) \simeq \frac{4\pi i}{\sqrt{8\pi\rho(z_o)}} e^{-i\pi/4} \sum_n |Q(\tilde{f})| \tilde{u}_n(z_o) \tilde{u}_n(z) \times \frac{\tilde{B}(s-\tilde{s}_n)}{\sqrt{\tilde{k}_{rn} r_o}} F_n(\tilde{f}), \tag{A6}$$

where

$$F_n(\tilde{f}) = \begin{cases} e^{i[\tilde{k}_{rn} r_o - \{2\pi\tilde{f}t - \angle Q(\tilde{f})\}/r_o + \mathrm{sgn}(\psi_n''(\tilde{f}))\pi/4]} \left[\dfrac{2\pi}{r_o \psi_n''(\tilde{f})} \right]^{1/2} & \text{if } \psi_n''(\tilde{f}) \neq 0, \\ e^{i[\tilde{k}_{rn} r_o - \{2\pi\tilde{f}t - \angle Q(\tilde{f})\}/r_o]} \left[\dfrac{6}{r_o |\psi_n'''(\tilde{f})|} \right]^{1/3} \dfrac{\Gamma(1/3)}{3} & \text{if } \psi_n''(\tilde{f}) = 0. \end{cases} \tag{A7}$$

The phase term of the source spectrum in Eq. (A3) can be eliminated when the time duration of the source is much smaller than the time spread of the source due to waveguide dispersion so that the relative phase difference is negligible. Equation (A3) then simplifies to

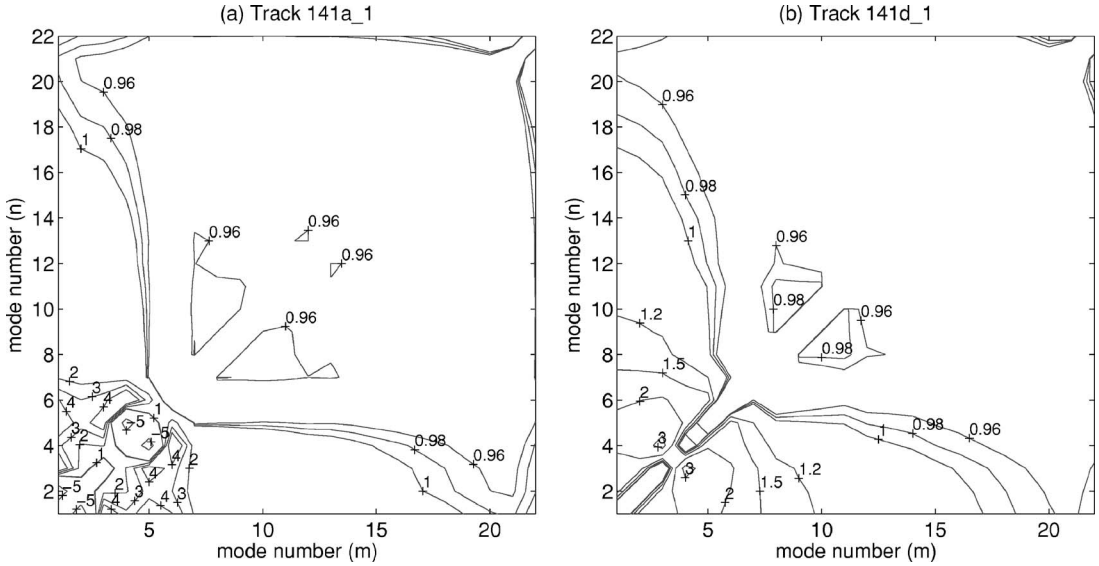

FIG. 24. (a) Track 141a_1: The waveguide invariant parameters β_{mn} calculated using the sound speed profile in Fig. 18(a) XBT2 at $f=415$ Hz. (b) Track 141d_1: The waveguide invariant parameters β_{mn} calculated using the sound speed profile in Fig. 18(b) XBT3 at $f=415$ Hz. It can be seen that roughly a factor of 2 change in β_{mn} has occurred in less than 2 hours.

$$P_{B+}(s,t) \simeq \frac{4\pi i}{\sqrt{8\pi\rho(z_o)}} e^{-i\pi/4} \sum_n |Q(\tilde{f})| \tilde{u}_n(z_o)\tilde{u}_n(z) \times \frac{\tilde{B}(s-\tilde{s}_n)}{\sqrt{\tilde{k}_{rn} r_o}} F_n(\tilde{f}) \tag{A8}$$

for $Q(f)=|Q(f)|$, where

$$F_n(\tilde{f}) = \begin{cases} e^{i(\tilde{k}_{rn} r_0 - 2\pi\tilde{f}t) - i\,\mathrm{sgn}(\tilde{v}'_{gn})\pi/4} \sqrt{\dfrac{(\tilde{v}_{gn})^2}{r_o|\tilde{v}'_{gn}|}} & \text{if } \tilde{v}'_{gn} \neq 0, \\ e^{i(\tilde{k}_{rn} r_0 - 2\pi\tilde{f}t)} \left[\dfrac{3(\tilde{v}_{gn})^2}{\pi r_o[\tilde{v}''_{gn}]} \right]^{1/3} \dfrac{\Gamma(1/3)}{3} & \text{if } \tilde{v}'_{gn} = 0. \end{cases} \tag{A9}$$

Similar results can be obtained if the received field is matched filtered with the transmitted signal. The matched filter output P_M of the beamformed field P_B is

$$P_M(s,t) = 2\,\mathrm{Re}\left\{ K \int_0^\infty P_B(s,f) Q^*(f) e^{-i2\pi ft} df \right\} = 2\,\mathrm{Re}\{P_{M+}(s,t)\}, \tag{A10}$$

where $K=[\int_{-\infty}^{\infty}|Q(f)|^2 df]^{-1/2}$. Again using the method of stationary phase,

$$P_{M+}(s,t) \simeq \frac{4\pi K i}{\sqrt{8\pi\rho(z_o)}} e^{-i\pi/4} \sum_n |Q(\tilde{f})|^2 \times \tilde{u}_n(z_o)\tilde{u}_n(z) \frac{\tilde{B}(s-\tilde{s}_n)}{\sqrt{\tilde{k}_{rn} r_o}} F_n(\tilde{f}), \tag{A11}$$

where $\tilde{f}$ satisfies Eq. (5). The function $F_n(\tilde{f})$ in Eq. (A11) is identical to that for impulsive sources given in Eq. (A9).

[1] C. S. Clay, "Array steering in a layered waveguide," J. Acoust. Soc. Am. **33**(7), 865–870 (1961).
[2] Y. Y. Wang, C. S. Clay, and E. C. Shang, "Bearing determination in a waveguide," J. Acoust. Soc. Am. **82**(1), 233–237 (1987).
[3] N. C. Makris and P. Ratilal, "A unified model for reverberation and submerged object scattering in a stratified ocean waveguide," J. Acoust. Soc. Am. **109**(3), 909–941 (2001).
[4] H. P. Bucker, "Use of calculated sound field and matched field detection to locate sound sources in shallow water," J. Acoust. Soc. Am. **59**, 368–373 (1976).
[5] A. B. Baggeroer, W. A. Kuperman, and H. Schmidt, "Matched field processing: Source localization in correlated noise as an optimum parameter estimation problem," J. Acoust. Soc. Am. **83**(2), 571–587 (1988).
[6] H. Schmidt, A. B. Baggeroer, W. A. Kuperman, and E. K. Sheer, "Environmentally tolerant beamforming for high-resolution matched field processing: Deterministic mismatch," J. Acoust. Soc. Am. **88**(4), 1851–1862 (1990).
[7] C. Feuillade, D. R. DelBalzo, and M. M. Rowe, "Environmental mismatch in shallow-water matched-field processing: Geoacoustic parameter variability," J. Acoust. Soc. Am. **85**(6), 2354–2364 (1989).
[8] G. B. Smith, H. A. Chandler, and C. Feuillade, "Performance stability of high-resolution matched-field processors to sound-speed mismatch in a shallow-water environment," J. Acoust. Soc. Am. **93**(5), 2617–2626 (1993).
[9] S. D. Chuprov, "Interference structure of a sound field in a layered ocean," in *Acoustics of the Ocean: Current Status (in Russian)*, edited by L. M. Brekhovskikh and I. B. Andreevoi (Nauka, Moscow, 1982), pp. 71–91.
[10] L. M. Brekhovskikh and Y. Lysanov, *Fundamentals of Ocean Acoustics*, 3rd ed. (Springer, New York, 2003).
[11] G. L. D'Spain and W. A. Kuperman, "Application of waveguide invariants to analysis of spectrograms from shallow water environments that vary in range and azimuth," J. Acoust. Soc. Am. **106**(5), 2454–2468 (1999).
[12] S. Lee and N. C. Makris, "A new invariant method for instantaneous source range estimation in an ocean waveguide from passive beam-time intensity data," J. Acoust. Soc. Am. **116**(4), 2646 (2004).
[13] S. Lee and N. C. Makris, "Range estimation of broadband noise sources in an ocean waveguide using the array invariant," J. Acoust. Soc. Am. **117**(4), 2577 (2005).
[14] L. E. Kinsler, A. R. Frey, A. B. Coppens, and J. V. Sanders, *Fundamentals of Acoustics*, 4th ed. (Wiley, New York, 2000).
[15] W. M. Ewing, W. S. Jardetzky, and F. Press, *Elastic Waves in Layered Media* (McGraw-Hill, New York, 1957).
[16] J. Miklowitz, *The Theory of Elastic Waves and Waveguides* (North–Holland, Amsterdam, 1978).
[17] P. Ratilal, "Remote sensing of submerged objects and geomorphology in continental shelf waters with acoustic waveguide scattering," Ph.D. thesis, Massachusetts Institute of Technology, Cambridge, MA, 2002.
[18] T. C. Yang, "Beam intensity striations and applications," J. Acoust. Soc. Am. **113**(3), 1342–1352 (2003).
[19] C. T. Tindle, "Virtual modes and mode amplitudes near cutoff," J. Acoust. Soc. Am. **66**(6), 1423–1428 (1979).
[20] R. J. Urick, *Principles of Underwater Sound*, 3rd ed. (McGraw–Hill, New York, 1983).
[21] F. J. Harris, "On the use of windows for harmonic analysis with the discrete Fourier transform," Proc. IEEE **66**(1), 51–83 (1978).
[22] N. C. Makris, "A foundation for logarithmic measures of fluctuating intensity in pattern recognition," Opt. Lett. **20**(19), 2012–2014 (1995).
[23] N. C. Makris, "The effect of saturated transmission scintillation on ocean acoustic intensity measurements," J. Acoust. Soc. Am. **100**(2), 769–783 (1996).
[24] M. Zanolin, I. Ingram, A. Thode, and N. C. Makris, "Asymptotic accuracy of geoacoustic inversions," J. Acoust. Soc. Am. **116**(4), 2031–2042 (2004).
[25] N. C. Makris, "Main acoustic clutter experiment cruise report," Technical Report, Office of Naval Research (2003).
[26] P. Ratilal, Y.-S. Lai, D. T. Symonds, L. A. Ruhlmann, J. A. Goff, C. W. Holland, J. R. Preston, E. K. Scheer, M. T. Garr, and N. C. Makris, "Long-range acoustic imaging of the continental shelf environment: The Acoustic Clutter Reconnaisance Experiment 2001," J. Acoust. Soc. Am. **117**(4), 1977–1998 (2005).
[27] C. M. Bender and S. A. Orszag, *Advanced Mathematical Methods for Scientists and Engineers* (McGraw–Hill, New York, 1978).